https://doi.org/10.5194/egusphere-2026-4173
Preprint. Discussion started: 1 September 2026

Thermodynamic and dynamic process attribution for Arctic sea ice loss during RILEs in CESM2

Annelies Sticker[1], François Massonnet[1], Thierry Fichefet[1], Alexandra Jahn[2,3], David A Bailey[4], and Benjamin Richaud[1]

[1]Earth and Life Institute, Earth and Climate, UCLouvain, Louvain-la-Neuve, Belgium
[2]Department of Atmospheric and Oceanic Sciences, University of Colorado Boulder, Boulder, CO, USA
[3]Institute for Arctic and Alpine Research, University of Colorado Boulder, Boulder, CO, USA
[4]Climate and Global Dynamics Laboratory, NSF National Center for Atmospheric Research, Boulder, CO, United States of America

Correspondence: Annelies Sticker (annelies.sticker@uclouvain.be)

Abstract. The decline in summer Arctic sea ice extent has been underway for several decades and is set to continue until summer Arctic sea ice disappears completely by the middle of the century, according to the latest climate projections. Based on observations and these climate projections, the rate of sea ice retreat is not linear: the decline in the Arctic sea ice cover is marked by periods of abrupt sea ice loss. Recent studies suggest that these rapid sea ice loss events (RILEs) will become increasingly likely in the coming decades. However, the processes driving RILEs remain poorly understood, in particular, the mechanisms controlling sea ice concentration evolution and the sources and sinks of sea ice mass during these climate events. Modeling tools that provide process-based analyses and budget decompositions across both historical and future climate simulations offer a robust framework for understanding the physical sources of these abrupt events. To investigate the processes behind these events, we characterize 31 September RILEs from the CESM2-lessmelt ensemble under the SSP3-7.0 forcing scenario across four periods spanning 1990–2065, and apply a two-stage process-based attribution framework to sea ice concentration and mass budget tendencies to identify the dominant mechanisms driving sea ice loss from a spatial perspective. RILEs are found to be a robust and recurrent feature of Arctic sea ice evolution, with a peak in occurrence around 2040, triggered across a wide range of initial sea ice states, from the thick and extensive cover of the early 1990s to the thin and reduced ice pack of the mid-21st century. Thermodynamic sea ice processes, and basal melt in particular, emerge as the dominant driver of the most intense and spatially significant sea ice losses during RILEs, while dynamic sea ice processes contribute a consistently minor fraction. Thermodynamic dominance strengthens as the century progresses and the ice pack thins, with dynamically dominated regions remaining confined to the vicinity of Greenland, the Canadian Archipelago, and the marginal ice zone. These results provide new process-level insight into the mechanisms of rapid summer Arctic sea ice loss and set the groundwork for the development of early warning indicators of the probability of RILE occurrence.

https://doi.org/10.5194/egusphere-2026-4173
Preprint. Discussion started: 1 September 2026

1 Introduction

The downward trend of the Arctic minimum sea ice extent (SIE) since the beginning of satellite observations is well known to be mainly associated with increases in greenhouse gas concentrations in the atmosphere (Stroeve and Notz, 2015; Meredith et al., 2019). However, superimposed on this long-term decrease are episodes of abrupt sea ice loss that occur on decadal-to-sub-decadal timescales and during which the rate of SIE decline substantially exceeds the contribution from the long-term forced signal alone (Kay et al., 2011; Swart et al., 2015; Baxter et al., 2019). As an example, September Arctic SIE retreated more than 4 times faster in the beginning of the 21st century (2003—2012: -2.27 million km^2/decade) than it did in the last decade (2016—2025: -0.5 million km^2/decade), while the long-term trend over 1979–2025 (-0.76 million km^2/decade) lies between these two values.

In addition, climate projections show that sea ice variability will intensify in the coming decades as the mean sea ice state becomes thinner, increasing the likelihood of extreme sea ice loss events, particularly when strong external forcing aligns with internally generated climate variations (Goosse et al., 2009; Mioduszewski et al., 2019). An expression of this variability are Rapid Ice Loss Events (RILEs), characterized by abrupt large-scale reductions in sea ice within a few years. Initially identified in climate model simulations (Holland et al., 2006), RILEs are plausible outcomes of the real Arctic sea ice evolution, with growing evidence supporting their potential occurrence in the near future (Döscher and Koenigk, 2013; Rogers et al., 2015; Auclair and Tremblay, 2018; Sticker et al., 2025). Moreover, the transition to a seasonally ice-free Arctic Ocean is likely to occur through the onset of a RILE rather than through a gradual decline (Heuzé and Jahn, 2024; Sticker et al., 2025). Regardless of whether a RILE will lead to an ice-free Arctic Ocean, such an event will have consequences for ecosystems (Arrigo and van Dijken, 2011; Wassmann et al., 2011; Post et al., 2013), and will cause changes in the wider Arctic climate (Lawrence et al., 2008; Wang et al., 2020) and even, potentially, in the mid-latitude atmospheric circulation regimes (Cohen et al., 2019; Delhaye et al., 2023).

Understanding the physical mechanisms underlying RILEs is therefore essential, both to improve our ability to anticipate their occurrence and to support the development of early warning systems. In particular, a better characterisation of the thermodynamic and dynamic contributions to sea ice area (SIA) loss during these events could provide valuable insight into the sources of predictive skill for seasonal-to-decadal sea ice predictions. The processes governing sea ice loss during RILEs remain largely unclear, with no consensus in the literature on the conditions that are necessary or sufficient to trigger them. A recurring framework is that RILEs require a preconditioned, fragile ice cover that is then susceptible to episodic anomalies in atmospheric circulation, moisture transport, or ocean heat input (Serreze et al., 2016; Årthun et al., 2019; Sumata et al., 2023). The proposed drivers span a wide range of processes, broadly categorised by their origin –internal climate variability versus externally forced change–, by the dominant physical component involved –atmosphere versus ocean– and by the nature of the underlying mechanism –dynamic versus thermodynamic (Holland et al., 2006; Döscher and Koenigk, 2013; Paquin et al., 2013; Polyakov et al., 2017; Auclair and Tremblay, 2018; Rieke et al., 2023). Preconditioning of the sea ice pack, surface

https://doi.org/10.5194/egusphere-2026-4173
Preprint. Discussion started: 1 September 2026

energy budget feedbacks, remote teleconnections, and the role of clouds and aerosols have also been identified as potentially important contributing factors (Holland et al., 2006; Vavrus et al., 2011; Paquin et al., 2013; Ding et al., 2014; Sticker et al., 2025). While the most likely drivers have already been identified in the literature, a quantified estimate of their relative contributions, the way they interplay and their necessary vs. sufficient roles in triggering rapid events, are still lacking. Notably, the occurrence of RILEs in the historical period suggests that a thin sea ice cover is not always a necessary precondition for their onset.

Several studies have explored the roles of thermodynamic and dynamic processes in Arctic sea ice variability and predictability (Bushuk et al., 2020; Polyakov et al., 2022; Guern-Lepage and Tremblay, 2023; Richaud et al., 2026). Polyakov et al. (2022) found that thermodynamic factors primarily drive seasonal predictability of Arctic sea ice thickness at large scales, while dynamic processes dominate regionally, and that their strong interaction complicates the identification of key drivers behind Arctic sea ice predictability. Bushuk et al. (2020) linked the May sea ice predictability barrier to the negative ice growth feedback, showing that predictability improves in spring when offshore ice motion creates SIC (sea ice concentration) anomalies amplified by the ice-albedo feedback, before summer advection reduces ice thickness predictability as SIC decreases. On the interannual timescale, sea ice lows are predominantly explained by thermodynamic processes, or by a combination of thermodynamic and dynamic processes, with the exception of the 2007 Summer Arctic sea ice minimum, which was primarily driven by dynamic processes (Richaud et al., 2026).

Beyond the usual thermodynamic vs. dynamic decomposition, the individual contributions of basal, surface, and lateral ice melt to sea ice loss remain less explored, particularly on decadal-to sub-decadal timescales. Studies have characterized the Arctic sea ice mass budget across the 21st century (Keen and Blockley, 2018; Keen et al., 2021) and during extreme events such as sea ice lows (Richaud et al., 2026), revealing a long-term increase in the importance of basal ice melt relative to surface and lateral ice melt. For sea ice lows specifically, Richaud et al. (2026) found that ice mass loss is predominantly driven by processes at the ice-ocean interface, either basal melt or reduced basal growth, with the exception of the anomalous summer of 2007. To our knowledge, no study has yet examined this finer decomposition of melt processes in the context of decadal-to-sub-decadal abrupt ice loss events such as RILEs.

In this study, we first characterize September RILEs in the CESM2-lessmelt ensemble by their temporal distribution, SIE trends, and sea ice thickness (SIT) evolution across four distinct periods. We then conduct a systematic process-level attribution of SIA loss during RILEs, decomposing the negative SIA trend at each grid cell into its thermodynamic and dynamic components to identify the dominant driver of local sea ice loss across the four periods. In a second stage, grid cells attributed to thermodynamic processes are further classified into basal and surface melt contributions based on the sea ice mass budget. The outline of the paper is organized as follows. Section 2 describes the CESM2 model and the CESM2-lessmelt ensemble, and introduces the attribution methodology. Section 3 presents the probability of RILEs in CESM2-lessmelt, their relationship to SIE anomalies relative to the ensemble mean, the evolution of SIT during RILEs, and the thermodynamic–dynamic attribu-

https://doi.org/10.5194/egusphere-2026-4173
Preprint. Discussion started: 1 September 2026

tion across the four periods, including the basal versus surface melt decomposition. Finally, section 4 discusses these results, synthesizes the dominant mechanisms of rapid Arctic sea ice loss, and section 5 summarizes the key findings and outlines perspectives for the development of early warning indicators of RILE occurrence.

2 Data and Methods

2.1 Model

This study relies on the CESM2-lessmelt ensemble (Kay et al., 2022), a modified version of the CESM2 Large Ensemble (Rodgers et al., 2021). CESM2 is a fully coupled Earth system model from the National Center for Atmospheric Research (NCAR) (Danabasoglu et al., 2020). The model uses CICE v5.1.2 for sea ice representation, featuring mushy-layer thermodynamics and a five-category ice thickness distribution (Hunke et al., 2013). However, CESM2 exhibits a systematic thin and low sea ice cover bias year-round, with sea ice volume (SIV) well below the PIOMAS reanalysis estimates throughout the historical period, and a summer SIE significantly lower than satellite observations, particularly in the East Siberian Sea (Schweiger et al., 2011). Despite these mean state biases, the model reproduces well the observed declining trends in Arctic SIE and SIV over 1979–2014 (DuVivier et al., 2020; Danabasoglu et al., 2020). Arctic near-surface air temperatures are better captured in CESM2 than in its predecessor, with the model broadly reproducing the regional characteristics of observed Arctic temperatures despite a remaining warm bias over the Arctic Ocean (McIlhattan and L'Ecuyer, 2025). As demonstrated by Massonnet et al. (2012), reproducing a correct sea ice state over recent decades is a necessary, though not sufficient, condition for models to reasonably anticipate future sea ice evolution. The standard CESM2-LE was therefore not used for this study, as its systematic sea ice biases would directly affect the characteristics of RILEs, whose characteristics, including their timing, duration, and triggering mechanisms, are closely tied to the background sea ice thickness and extent. The use of CESM2-lessmelt, which corrects the bias of CESM2 toward insufficient late-summer Arctic sea ice cover through targeted parameter adjustments (Kay et al., 2022), provides a closer representation of the Arctic sea ice state towards observations.

The changes in CESM2-lessmelt simulations include an increase in the snow melt onset temperature and an increase in the albedo of snow on sea ice (Kay et al., 2022). Firstly, the melt onset temperature was increased from -1.5°C to -1.0°C. This parameter directly dictates when snow grains begin to grow from a dry snow state to a melting snow state. By raising this temperature threshold, the model delays the initiation of snowmelt, thereby extending the period during which snow remains frozen on the sea ice surface. Secondly, the dry snow grain radius was reduced from 187.5 µm to 125 µm, which increases the effective dry snow albedo from approximately 0.88 to 0.90. A smaller snow grain radius scatters incoming solar radiation more efficiently, leading to higher snow albedo. Both modifications, the delayed snowmelt onset and increased snow albedo, work together to reduce surface sea ice melt, hence the name CESM2-lessmelt, leading to a thicker and more resilient sea ice cover. These changes are realized without degrading the global simulation including top-of-atmosphere energy balance, surface temperature, surface precipitation, and major modes of climate variability (Kay et al., 2022).

We analyze simulations under CMIP6 historical forcing from 1990 to 2014 and under the medium-to-high emission SSP3-7.0 scenario from 2015 to 2100 (Fig. 1). The CMIP6 historical forcing prescribes an abrupt increase in biomass burning (BB) emission variability during 1997–2014, which induces excessive Northern Hemisphere warming and a spurious Arctic sea ice loss-and-recovery signal over 1997–2025 (Fasullo et al., 2022; DeRepentigny et al., 2022). CESM2 is particularly sensitive to this discontinuity. Five members of the CESM2-lessmelt ensemble (118–122) therefore use the smoothed BB (smbb) configuration (DeRepentigny et al., 2022), in which BB emissions are smoothed over 1990–2020 to dampen this signal, while the remaining four members (112–115) follow the standard CMIP6 forcing. All nine members are used throughout this study. To investigate RILEs throughout the 21st century, we divide the study period into four sub-periods. The first, referred to as the early period (1990–2014), is based on historical simulations. The remaining three sub-periods draw on future projections under the SSP3-7.0 forcing scenario: the mid-early period (2015–2030), covering the near-present; the mid-late period (2030–2045), representing the close future; and the late period (2045–2064), corresponding to the emergence of a seasonally sea ice-free Arctic Ocean. The smoothing period (1990–2020) overlaps with both the early (1990–2014) and mid-early (2015–2029) analysis periods, which may influence results for these two periods.

Sea ice outputs analyzed in this study include Arctic SIE, SIC, SIV, and SIA partitioned by thickness categories, with a focus on September RILEs. To characterize the processes driving sea ice loss during the melt season (April–August), we examine sea ice concentration and mass budgets through process-attributed variables: sea ice concentration changes due to thermodynamic (*sidconcth*) and dynamic (*sidconcdyn*) processes, sea ice mass changes due to thermodynamic (*sidmassth*) and dynamic (*sidmassdyn*) processes, and sea ice mass changes due to basal melt (*sidmassmeltbot*) and surface melt (*sidmassmelttop*) processes. By convention, negative tendencies indicate sea ice mass loss (Fig. S2). To gain deeper insight into the processes occurring during an abrupt sea ice loss event, we also look at SIA partitioned by thickness categories. This is done by analyzing the variable *siitdconc*, which provides the fractional area of sea ice coverage per thickness category. This variable quantifies the proportion of a grid cell's area covered by sea ice, distributed across different ice thickness categories. In the sea ice model, the ice thickness distribution (ITD) is discretized into five categories (Bitz et al. (2001)). The five thickness categories follow the boundaries defined by Lipscomb (2001): cat.1: 0.00–0.64 m, cat.2: 0.64–1.39 m, cat.3: 1.39–2.47 m, cat.4: 2.47–4.57 m, and cat.5: $>$4.57 m.

2.2 RILE detection

We define a RILE as a period lasting at least 4 years, during which the trend in the 5-year running mean minimum SIE is lower or equal to -0.3 million km^2 per year, and apply this definition to the nine CESM2-lessmelt members (Auclair and Tremblay, 2018; Sticker et al., 2025). Applying this definition year-round, a total of 156 RILEs are detected across all months over the full 1990–2064 period in the CESM2-lessmelt ensemble. Focusing on September, a total of 31 RILEs are identified over the 1990–2064 period, distributed across the four defined periods as follows: 9 in the early period (1990–2015), 6 in the mid-early period (2015–2030), 10 in the mid-late period (2030–2045), and 6 in the late period (2045–2065). Notably, all RILEs identified

https://doi.org/10.5194/egusphere-2026-4173
Preprint. Discussion started: 1 September 2026

in the final period from 2045–2065 result in September SIE reaching ice-free Arctic Ocean conditions. All ensemble members exhibit at least one RILE, with a maximum of five RILEs detected in a single member. Among the 9 RILEs identified in the early period, 6 occur in members using the standard CESM2 BB emission forcing, while the remaining 3 are found in members employing the smbb modification.

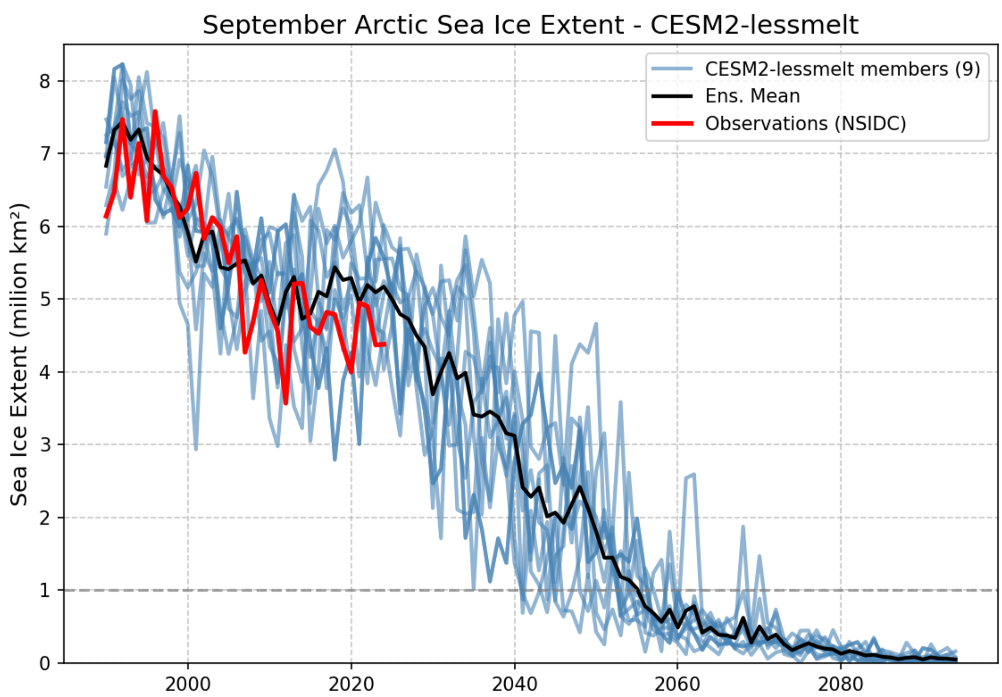

Figure 1. September Arctic sea ice extent for 9 members of CESM2-lessmelt, timeseries 1990-2100. Observations are from NSIDC sea ice index (Fetterer et al., 2017) with area pole-filling.

2.3 Thermodynamic and dynamic attribution for sea ice loss during RILEs

A two-stage attribution framework is developed to identify the dominant processes responsible for September SIC decline during RILEs. Specifically, the framework aims to disentangle the relative contributions of thermodynamic vs. dynamic processes during the RILE at the grid-cell level. To this end, a quantitative comparison is made between the decline in September SIC over the RILE period, which reflects the time evolution of the sea ice state, and the trend in the seasonally integrated SIC tendency terms, which reflect the time evolution of SIC tendency due to process specific drivers during the RILE. The SIC tendency terms (and their decomposition into thermodynamical vs. dynamical processes) are available as standard outputs in

https://doi.org/10.5194/egusphere-2026-4173
Preprint. Discussion started: 1 September 2026

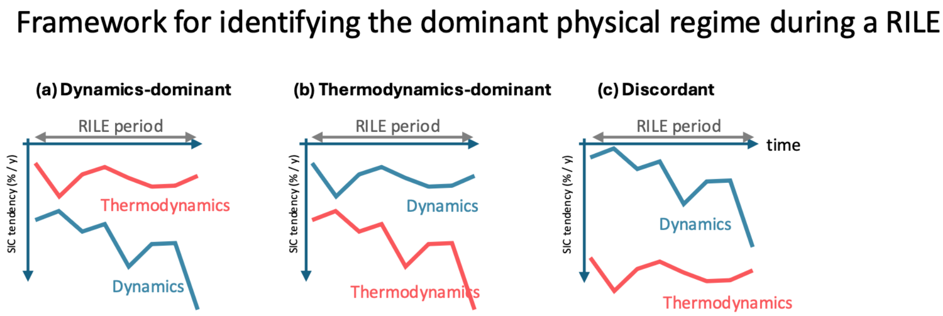

Figure 2. Schematic illustration of the attribution categories used in this study. Each panel shows the temporal evolution of the SIC tendency (% yr^{-1}) due to thermodynamic (red) and dynamic (blue) processes over the course of a RILE. (a) Dynamics-dominant: dynamic processes drive both the accelerating trend and the largest integrated sea ice loss. (b) Thermodynamics-dominant: thermodynamic processes dominate both the trend and total loss. (c) Discordant: the process driving the accelerating trend differs from the process dominating the total integrated sea ice loss.

the CESM2-lessmelt experiments analyzed here.

A strong correspondence is found across all RILEs between trends in September SIC and trends in the April-August integrated SIC tendency (r=0.83-0.93, depending on the RILE considered). This relationship is expected, since the SIC state in September is, by definition, the time integral of the SIC tendency over the melting season plus the initial winter (March) state:

$$\frac{d\mathrm{SIC}_{\mathrm{Sep}}}{dt} - \frac{d\mathrm{SIC}_{\mathrm{Mar}}}{dt} = \frac{d}{dt} \int\limits_{\text{melt season}} \mathrm{sidconc}\, dt' \tag{1}$$

where $\frac{d}{dt}$ denotes the linear trend estimated over the duration of the RILE, and $\mathrm{sidconc} = \mathrm{sidconcth} + \mathrm{sidconcdyn}$ is the total sea ice concentration tendency, with contributions from thermodynamic ($sidconcth$) and dynamic ($sidconcdyn$) processes.

Alongside relating the total SIC trend to the two drivers, we also examine the relationship between the drivers themselves. We find that, over the identified RILEs, the evolution of SIC tendency due to thermodynamic processes is strongly anticorrelated with the evolution of SIC tendency due to dynamic processes (r=-0.82 to -0.74 across the domain, depending on the RILE), indicating that the two processes play highly complementary roles. In regions of strong ice export or divergence, ice is thinner and open water increases, creating favorable conditions for late-winter and early-spring basal and lateral ice growth. Conversely, in areas of convergence, the thicker ice pack is more susceptible to surface or bottom melting.

Based on these trends, the grid cells are categorized into three possible categories: (a) dynamics-dominant, (b) thermodynamics-dominant and, (b) discordant (Fig. 2). A grid cell is categorized as "dynamics-dominant" if the following conditions are simu-

https://doi.org/10.5194/egusphere-2026-4173
Preprint. Discussion started: 1 September 2026

latenously met: (i) the SIC tendency from dynamics becomes significantly more negative over the course of the RILE, with a net change below -0.1%/year; (ii) the time evolution of SIC tendency from dynamics explains more than 20% of the SIC trend during the RILE; (iii) the SIC tendency from dynamics is, during the RILE, more negative than the SIC tendency from thermodynamics; and (iv) the total sea ice loss due to dynamic processes integrated over the melt season (April–August) exceeds that due to thermodynamic processes. In that case, the role of dynamical processes increases during the RILE in a region where it is already predominant, and it primarily explains the SIC change; the RILE is therefore labelled as "dynamics-dominant" for that grid cell (Fig. 2a). Likewise, a grid cell is categorized thermodynamics-dominant" (Fig. 2b) following the same reasoning but swapping the roles of dynamics and thermodynamics. A grid cell is categorized as "discordant" when one type of process (e.g., dynamics) explains the SIC trend during the RILE and increases in importance over the course of the RILE, satisfying conditions (i), (ii), and (iii) above, but the other type of process remains more important in absolute terms, i.e., condition (iv) (Fig. 2c). This twofold approach allows us to identify both which process dominates total sea ice loss and which process is increasingly contributing to it, thereby gaining importance over the course of the RILE.

To summarize, the dynamics-dominant category indicates regions where dynamics exert a strong control on SIC loss and where their effect is amplified during a RILE, suggesting regions where ice divergence and advection are the primary mechanisms of ice loss. The thermodynamics-dominant category indicates regions where thermodynamics exert a strong control on the SIC loss and where their effect is amplified during a RILE, thus identifying regions where basal and surface melting driven by oceanic and atmospheric fluxes predominantly dominate ice loss. The discordant category corresponds to a transitional state where thermodynamics take an increasing role (e.g. through the ice-albedo feedback) in a background state marked by strong dynamics-induced sea ice loss, or where the dynamics play an increasing role (e.g. through mechanical weakening) in a background state marked by strong thermodynamics-induced sea ice loss.

The thermodynamic and dynamic decomposition of SIC changes offers a first-order picture of the processes involved in RILEs, but a more complete understanding requires going further, by extending it to sea ice mass changes and, especially, isolating the contributions of surface and basal melt within the thermodynamic component. Sea ice loss can occur without any noticeable change in area, for instance, when ice thins progressively without retreating. Conversely, area can decrease without mass loss, due to ridging or rafting of sea ice. Therefore, area-based metrics may underestimate or misattribute the true magnitude of thermodynamics and dynamics processes. Incorporating sea ice mass allows us to better constrain the relative contributions of dynamic and thermodynamic to the overall sea ice loss during RILEs. We therefore examine trends and total changes in sea ice mass loss attributed to thermodynamic and dynamic processes, following the same approach as for sea ice concentration changes.

Our framework refines these primary attributions based on concentration changes through two distinct pathways depending on the initial classification. For cells attributed to thermodynamic dominance, we subdivide the thermodynamic contribution into surface versus basal melt processes. A cell is classified as surface-melt dominant if the surface melt trend is negative,

https://doi.org/10.5194/egusphere-2026-4173
Preprint. Discussion started: 1 September 2026

stronger than basal melt, and accounts for a larger absolute contribution to sea ice loss. Basal melt dominance is established through symmetric criteria. If neither melt type clearly dominates, the cell retains its thermodynamic classification without further subdivision. For cells initially classified in the discordant category, we apply a mass-based reattribution procedure to complement the area-based attribution. If thermodynamic mass changes show negative trends, dominate over dynamic trends, and contribute more in absolute terms, the cell is reattributed to the first category (thermodynamics-dominant), and subjected to the surface/basal melt subdivision. Similarly, if dynamic mass changes meet similar criteria, the cell is reattributed to the second category (dynamics-dominant). If neither process achieves mass-based process dominance, the cell remains in its original discordant category, indicating a contribution from both processes or a weaker signal in the sea ice loss.

Final attribution maps are constructed by aggregating the individual cell-level attribution results across all RILEs belonging to a given period, using a frequency-based approach combined with a binomial significance test. For each September RILE in the ensemble, every Arctic grid cell is assigned an attribution category based on the two stage method decomposition framework. Then, for each grid cell, the frequency of occurrence of each attribution category is computed across all RILEs within the period. Cells for which fewer than 50% of the RILEs in the period detected a negative trend are excluded from the composite. Among the remaining cells, the category with the highest frequency of occurrence is assigned as the composite attribution; cells where two or more categories occur with equal frequency are assigned to a "no consensus" category. The robustness of the dominant category is assessed using a one-sided binomial significance test, under the null hypothesis that occurrences are distributed uniformly among the number of categories observed at a given cell. A cell is considered to exhibit a statistically significant dominant attribution when the p-value falls below 0.05 and the dominant category accounts for more than 50% of the contributing RILEs; such cells are marked with black dots on Fig. 7 and Fig. 9. The statistical significance of this test is inherently limited by the small number of RILEs per period, ranging from 6 to 10.

3 Results

3.1 Likelihood of RILEs

We characterize the probability of occurence of a RILE as the fraction of members experiencing a RILE in a given year, computed over 1990–2100 for CESM2-LE (50 members, Fig. 3a) and CESM2-lessmelt (9 members, Fig. 3b). RILEs occur predominantly between July and December throughout the simulation run, with a probability peak around 2040 in CESM2-lessmelt in September. This result not only identifies the most likely timing for a RILE in CESM2-lessmelt but also highlights that RILEs can occur as early as the 1990s–2000s during summer months, well before the probability peak around 2040. The presence of such early events raises questions about the respective roles of external forcing and internal preconditioning in triggering RILEs. While forcing sets the long-term trajectory of sea ice loss, early occurrences suggest that a favorable triggering event alone may be sufficient to initiate a RILE. In CESM2-LE, the peak of probability occurs around 2000 and corresponds to a notable acceleration in sea ice decline linked to increased variability in prescribed BB emissions driven by summertime aerosol-cloud interactions according to DeRepentigny et al. (2022) linked with lower than observed sea ice extent.

https://doi.org/10.5194/egusphere-2026-4173
Preprint. Discussion started: 1 September 2026

The second peak of RILE probability arise around 2025 for CESM2-LE, still 15 years earlier than CESM2-lessmelt simulations that are showing a more realistic Arctic sea ice mean state.

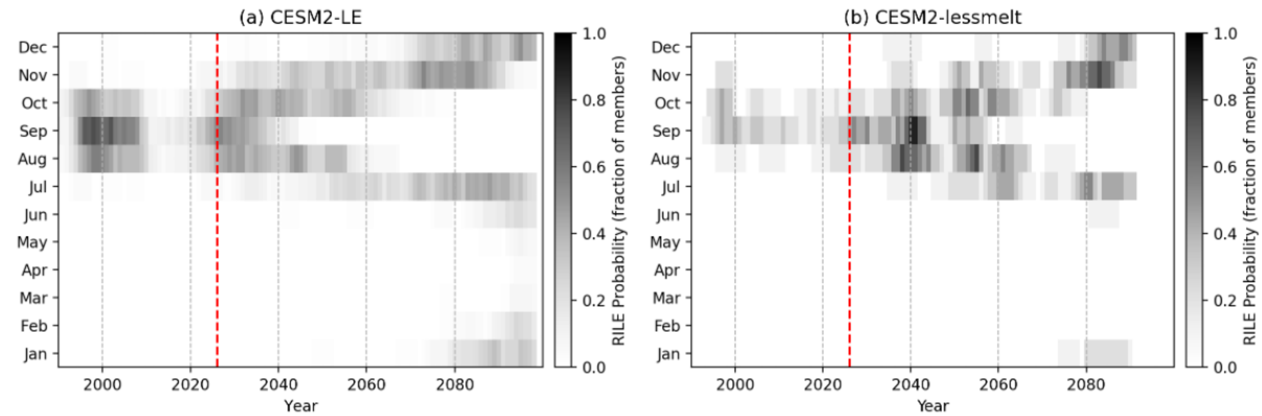

Figure 3. Density of RILE occurrence by month and year for (a) CESM2-LE (50 members) and (b) CESM2-lessmelt (9 members), both under the SSP3-7.0 emission scenario over 1990–2100. For each month and year, the density is computed as the fraction of ensemble members experiencing a RILE. CESM2-LE is included here for comparison purposes only, to illustrate how correcting the systematic sea ice bias in CESM2 toward insufficient late-summer Arctic sea ice cover shifts the timing and distribution of RILEs toward a more realistic representation. The analysis in the remainder of the paper is based exclusively on CESM2-lessmelt. The dotted red vertical line indicates the year 2026.

The role of internal variability in RILE onset is important to consider. If a RILE is primarily internally driven, it could appear as a transient departure from the mean state, with the system subsequently recovering, manifesting as an abrupt event in SIE. To investigate whether RILEs represent a response attempting to return to the system's mean state (Fig. 1, black line), we calculate the SIE anomaly at the onset of each RILE relative to the ensemble mean (Fig.4, blue bars). While the majority of RILEs initiate under positive anomaly conditions compared to the ensemble mean, nearly a quarter begin with negative anomalies with respect to the ensemble mean. Across all 156 RILEs detected year-round in CESM2-lessmelt, 77.6% begin with a positive anomaly; however, half of the RILEs have a positive anomaly between 0 and 1 million km^2, while the 27.6% left exceed 1 million km^2. The remaining 22.4% begin with negative anomalies; however, Fig. 4 reveals that these are not only a minority but also clustered very close to the ensemble mean (0 to -1.75 million km^2), making them effectively near average onset conditions as well. This is even more pronounced for September RILEs, where negative anomalies represent only 13% of cases and remain within 0 to -0.25 million km^2 of the mean. Moreover, a non-negligible fraction (38.8%) of September RILEs begin with strongly positive anomalies exceeding 1 million km^2 (Fig. 4, blue bars). Taken together, these findings indicate that RILEs predominantly initiate when SIE is near or above the ensemble mean, with only a small minority beginning under slightly below-average conditions.

https://doi.org/10.5194/egusphere-2026-4173
Preprint. Discussion started: 1 September 2026

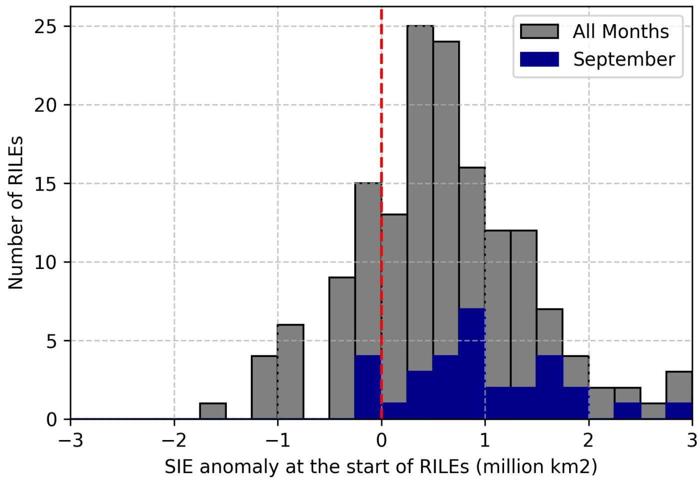

Figure 4. Sea ice extent anomaly compared to ensemble mean at the onset of RILEs from CESM2-lessmelt ensemble over the period 1990-2095 for all months in grey and September only in dark blue. The red dashed line marks zero anomaly, i.e. the ensemble mean.

3.2 Beyond sea ice concentration: the role of thickness in RILEs

RILEs are not only characterized by abrupt SIE decreases but also by abrupt SIV decreases. Among the 31 September RILEs of the 9 CESM2-lessmelt members, some RILEs not only exhibit strong negative trends in SIE, but also show substantial declines in SIV, with trends from -0.7 to -2.6 $\times 10^3$ km^3/yr in the early period with a median SIV loss of 1.2$\times 10^3$ km^3/yr (Fig. 5). In contrast, the late period displays RILEs with much weaker volume trends (-0.2 to -0.5 $\times 10^3$ km^3/yr), suggesting that these are primarily extent-driven rather than volume-driven events. The mid-periods reveal a transitional trend in SIV loss between the early and late phases, with the median rate shifting from -1$\times 10^3$ km^3/yr (mid-early) to -0.4$\times 10^3$ km^3/yr (mid-late). The early period exhibits the highest variability in SIV trends alongside the strongest rate of volume decline, yet paradoxically shows the lowest variability and least negative SIE trends. In contrast, SIE trend severity and variability increase through the mid periods before stabilizing in the late period, while SIV trends follow the opposite trajectory, becoming progressively lower toward the late period.

This diversity in SIV trends across events motivates a closer examination of how SIT is distributed and evolves during RILEs. Our analysis shows that in the early periods, RILEs involve both a decline in total SIA and a redistribution of ice toward thinner thickness categories, while in later periods, as the ice pack has already thinned, RILEs are dominated primarily by large area losses with little remaining thickness redistribution to occur. To analyze this behavior, we first examine the SIA by thickness category and its evolution throughout the century from 1990 to 2065. Over the course of the century, the nine simulations exhibit remarkably similar trends. In the early 1990s, the fractional area of sea ice, defined here as the proportion of total

https://doi.org/10.5194/egusphere-2026-4173
Preprint. Discussion started: 1 September 2026

SIA occupied by each thickness category, is relatively evenly distributed across categories. Starting in the 2000s, however, the thinnest category (cat. 1, 0.00-0.64m) begins to dominate, increasing from a minor fraction to between 40% and 60% of total SIA, while thicker categories occupy a progressively reduced share (Fig. S1). As the Arctic approaches near ice-free conditions by the mid-21st century, the total SIA shrinks to the point where all thickness categories, including the thinnest ones, occupy similarly small fractions, reflecting the near-complete disappearance of the ice pack.

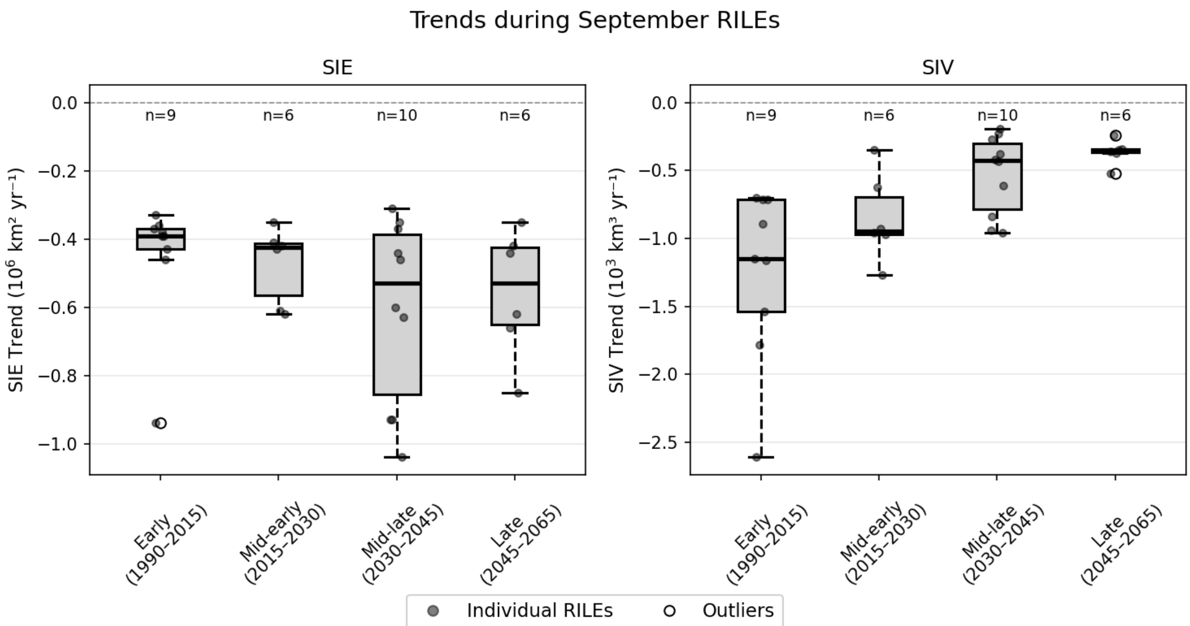

Figure 5. Boxplots of September SIE (left, $10^6\mathrm{km}^2\mathrm{y}^{-1}$) and SIV (right, $10^3\mathrm{km}^3\mathrm{y}^{-1}$) trends during RILEs across four periods: early(1990–2015, n=9), mid-early (2015–2030, n=6), mid-late (2030–2045, n=10), late(2045–2065, n=6), where n is the number of RILEs per period. The box spans the interquartile range (IQR, 25th–75th percentile), with the horizontal line indicating the median; whiskers extend to 1.5 times the Interquartile Range, and open circles denote outliers beyond this range. Individual RILEs are shown as filled circles. The dashed horizontal line at zero is shown for reference.

The evolution of the SIT distribution during RILEs reveals distinct characteristics across the four periods. In the early period (1990–2014), RILEs begin with a mean total area of 5.1 million km^2 distributed relatively uniformly across thickness categories, and end with a marked redistribution toward thinner ice: the thinnest category (cat. 1, SIT < 0.64 m) increases its fractional contribution by more than 10%, while total area decreases marginally (Fig. 6). All other categories decrease both in fractional contribution and total area, with category 3 (1.39–2.47 m) experiencing the largest fractional loss, declining from $19 \pm 6\%$ to $12 \pm 3\%$ of total SIA (mean $\pm$ standard deviation across RILEs within the period). This indicates that during early-period RILEs, sea ice is primarily redistributed from thicker to thinner categories or lost during the RILE period. The mid-early period (2015–2030) follows a similar pattern but with a thinner sea ice state compared to the early period, with

https://doi.org/10.5194/egusphere-2026-4173
Preprint. Discussion started: 1 September 2026

category 1 expanding from a mean start area of 37% to nearly half of the total ice-covered area as thicker categories progressively diminish. In contrast, the mid-late (2030–2045) and late (2045–2064) periods are characterized by substantial area losses across all thickness categories, especially the thinnest category that represents more than half of the sea ice area, rather than redistribution, driving the system toward near ice-free conditions in the mid-late period and fully ice-free conditions in the late period, with total area dropping below 1 million km^2. This shift in the thickness distribution of the ice being lost reflects the overall thinning of the Arctic ice pack over time and explains the weaker volume decline observed during the later events, when the initial SIV is already lower ($\sim$3 $\times 10^3 \mathrm{km}^3$).

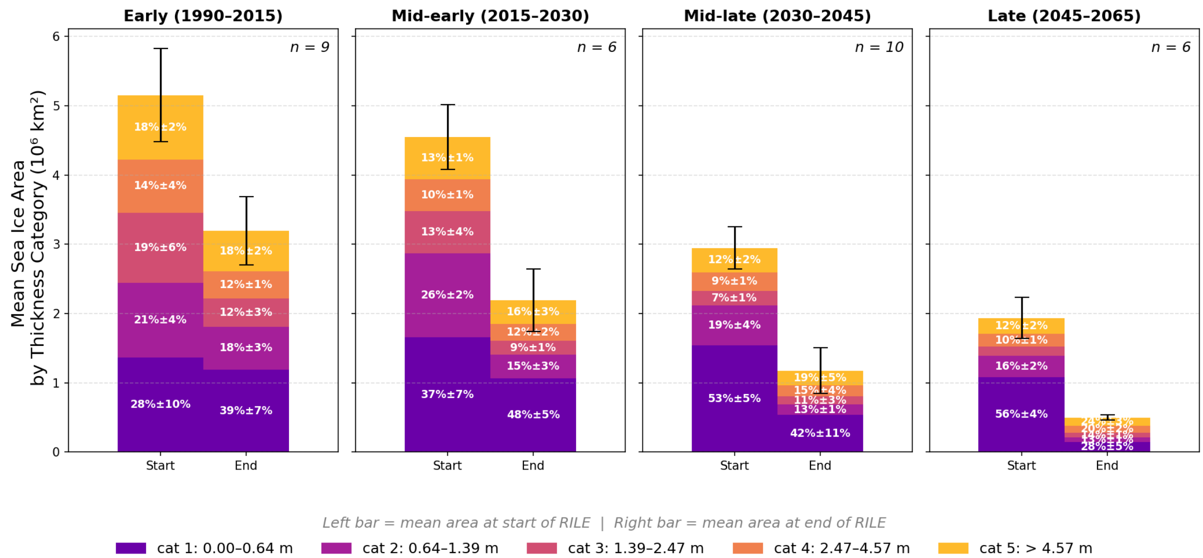

Figure 6. Mean and standard deviation of Arctic SIA by thickness categories at the start (left bars) and end (right bars) of RILEs across four periods; early period (1990-2015), mid-early period (2015-2030), mid-late period (2030-2045) and late period (2045-2065). Each color represents a thickness category ranging from thin ice (<0.64 m) to very thick ice (>4.57 m). Percentages within the bars indicate the contribution of each category to the total SIA. Black error bars represent the standard deviation of the total sea ice area (sum of all thickness categories) across RILEs within each period.

3.3 Mechanisms driving sea ice decline during RILEs

3.3.1 First-stage attribution: concentration-based

The preceding analysis establishes the large-scale characteristics of RILEs in terms of SIE, volume, and thickness distribution. While sea ice state variables characterize how RILEs unfold, they do not allow one to pinpoint why the sea ice cover changes the way it does, specifically, whether a given change in concentration or mass is driven by thermodynamic or dynamic processes. We now shift focus from characterising what the ice cover looks like during these events to understanding where sea

https://doi.org/10.5194/egusphere-2026-4173
Preprint. Discussion started: 1 September 2026

ice is lost and which processes are responsible, by applying a process-based attribution method (see Sect. 2.3) decomposing SIC changes into their thermodynamic and dynamic contributions.

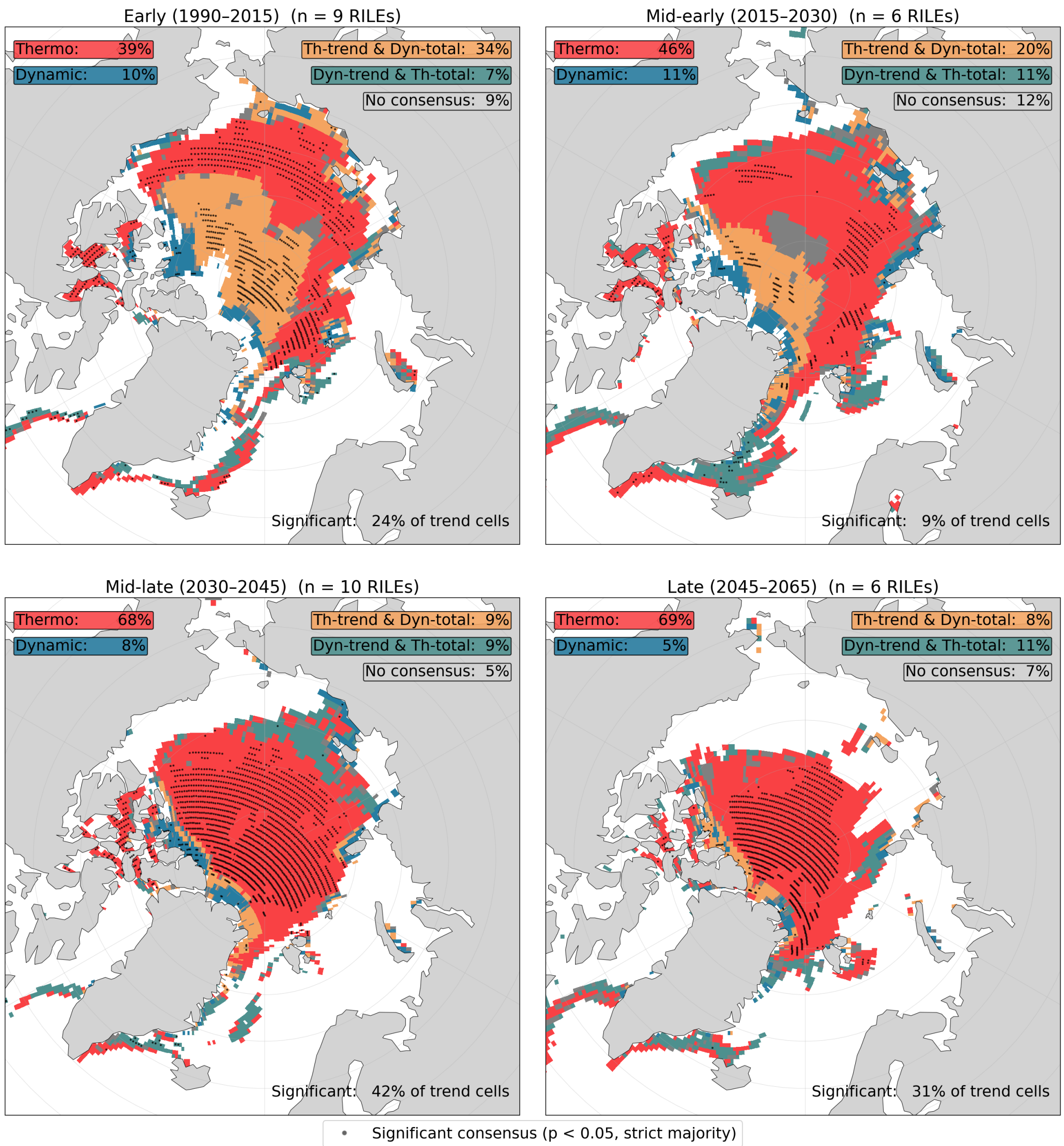

Figure 7. Composite attribution maps of Arctic SIC trends during September RILEs for each period. At each grid cell, the dominant attribution category is determined by the majority across all RILEs within the period, provided that at least 50% of RILEs show a negative SIC trend at that cell. Black dots indicate cells where the majority winner is statistically significant (binomial test, $p < 0.05$). Grey cells indicate no consensus among RILEs. n denotes the number of RILEs in each period.

https://doi.org/10.5194/egusphere-2026-4173
Preprint. Discussion started: 1 September 2026

The attribution maps of SIC change due to thermodynamic and dynamic processes only (Fig. 7) reveal a consistent dominance of thermodynamic processes across all four RILE periods, with thermodynamics-attributed regions accounting for 39% to 69% of grid cells experiencing September sea ice decline. Dynamic processes contribute to 5% to 11% of the grid cells, while the discordant category (Th/Dyn-total & Dyn/Th-total in Fig. 7) represents 18% to 41% of the total, the rest in grey shows no-consensus zone where variability is high between RILEs of the same period.

The temporal evolution of attribution categories reveals an increase of thermodynamics dominance in later RILEs. Thermodynamic attribution increases from 39% (early period) to 69% (mid-late and late periods), primarily because discordant (th-trend & dyn-total) regions from early and mid-early periods become thermodynamically attributed in later periods. In the early periods, thermodynamic dominance is concentrated in the marginal seas, from the Beaufort Sea to the region north of Svalbard, before expanding toward the central Arctic Ocean and eventually north of Greenland in the late periods. By the latest period, this central region represents the only remaining area of sea ice, as the marginal seas have become seasonally ice-free. Discordant categories exhibit contrasting temporal patterns. The th-trend & dyn-total category, in which dynamic processes dominate the total sea ice loss while thermodynamic processes show a stronger accelerating trend, accounts for 34% of the declining sea ice area in the early period and 20% in the mid-early period, appearing predominantly in a region near the North Pole and close to Greenland. By mid-late to late periods, this category reduces to 8-9%, persisting along north of Greenland in the Lincoln Sea and in the proximity of the Canadian Arctic Archipelago. In contrast, the dyn-trend & th-total category, in which thermodynamic processes dominate absolute ice loss but dynamic trends are accelerating, increases from 7% of the area in the historical period to 9-11% in later periods. This category appears primarily in marginal ice zones. The expansion of this category suggests that, as the ice pack thins and becomes more mobile, dynamic processes gain importance and become comparable to thermodynamic processes. In contrast, pure dynamic attribution declines from RILEs in the early to late period, a trend that could be explained by the increase of thermodynamic role: regions previously dominated exclusively by dynamics transition to mixed-process regimes, where both thermodynamic melting and ice advection contribute substantially. Dynamically dominated regions remain spatially consistent across all four periods, confined to north of Greenland and the Canadian Archipelago and along the margins of the ice pack.

The statistical significance of attribution maps within each period is assessed as described in Sect. 2.3. The fraction of significantly attributed grid cells ranges from 9% in the mid-early period to 42% in the mid-late period, with the lower value in the mid-early period likely reflecting greater spatial variability across RILEs. Across all four periods, thermodynamically dominated regions consistently show the highest significance, while discordant regions – where dynamic processes dominate the total sea ice loss – also exhibit significant grid cells, particularly in the earliest period.

Since sea ice loss is not spatially uniform across the Arctic, we assess the distribution of September SIC trends across grid cells categorized into thermodynamically dominated, dynamically dominated, and discordant regions (grouping both discordant categories). For each of the 31 RILEs, we pool the SIC trends of all grid cells belonging to each category and represent

https://doi.org/10.5194/egusphere-2026-4173
Preprint. Discussion started: 1 September 2026

their distributions as probability density functions (Fig. 8). Across all four periods, thermodynamically dominated regions consistently exhibit the most severe SIC trends, while dynamically dominated and discordant regions are associated with trends closer to zero. This indicates that thermodynamic processes are not only the dominant driver of total SIA loss during RILEs, but also the process most strongly associated with the most intense local SIC decline. In the early and both mid-periods, the mean SIC trend in thermodynamically dominated regions is approximately -8.8% yr^{-1} (early and mid-early) and -8.4% yr^{-1} (mid-late), substantially more negative than in dynamically dominated regions (-5.1 to -5.7% yr^{-1}) and discordant regions (-4.6 to -6.7% yr^{-1}). In the late period, the distributions of thermodynamic and dynamic regions converge, with means of -7.8 and -7.1% yr^{-1}, respectively. The reduction in the fraction of very negative trend cells in the late period, despite continued overall sea ice decline, is consistent with a thinner and less extensive ice pack in which extreme local trends become less spatially prevalent. As the ice retreats, there is less area over which intense melt can occur.

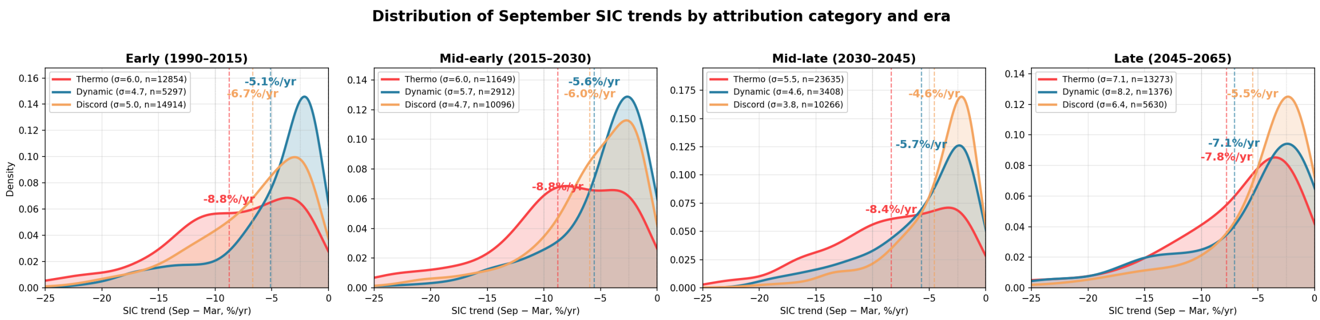

Figure 8. Probability density functions of September SIC trends by attribution category across the four periods: early (1990–2015), mid-early (2015–2030), mid-late (2030–2045), and late (2045–2065). Each distribution pools area-weighted SIC trends from all grid cells attributed to thermodynamic (red), dynamic (blue), and discordant (orange) categories across all RILEs within the period. Dashed vertical lines indicate the mean of each distribution. Values of σ and n in the legend denote the standard deviation and the total number of grid cells, respectively.

3.3.2 Second-stage attribution: sea ice mass-based

In this section, we refine the four concentration-based attribution categories by incorporating the sea ice mass budget and decomposing the thermodynamic component into its surface and basal melt contributions. Two additional categories are introduced: one for grid cells where sea ice decline during the RILE is dominated by basal melt (Fig. 9, orange), and one where surface melt is the dominant process (Fig. 9, yellow). Basal melt refers to ice loss at the ice-ocean interface, and tends to dominate in regions where warm Atlantic or Pacific water masses, though subducted below the surface, progressively release heat upward to the ice base, or where surface waters in recently ice-free areas warm through atmospheric heating and albedo feedback. Surface melt, in contrast, occurs at the ice-atmosphere interface and is primarily driven by absorbed shortwave, longwave radiation, and turbulent heat fluxes from the atmosphere, becoming particularly active during summer months when solar insolation is at its peak.

https://doi.org/10.5194/egusphere-2026-4173
Preprint. Discussion started: 1 September 2026

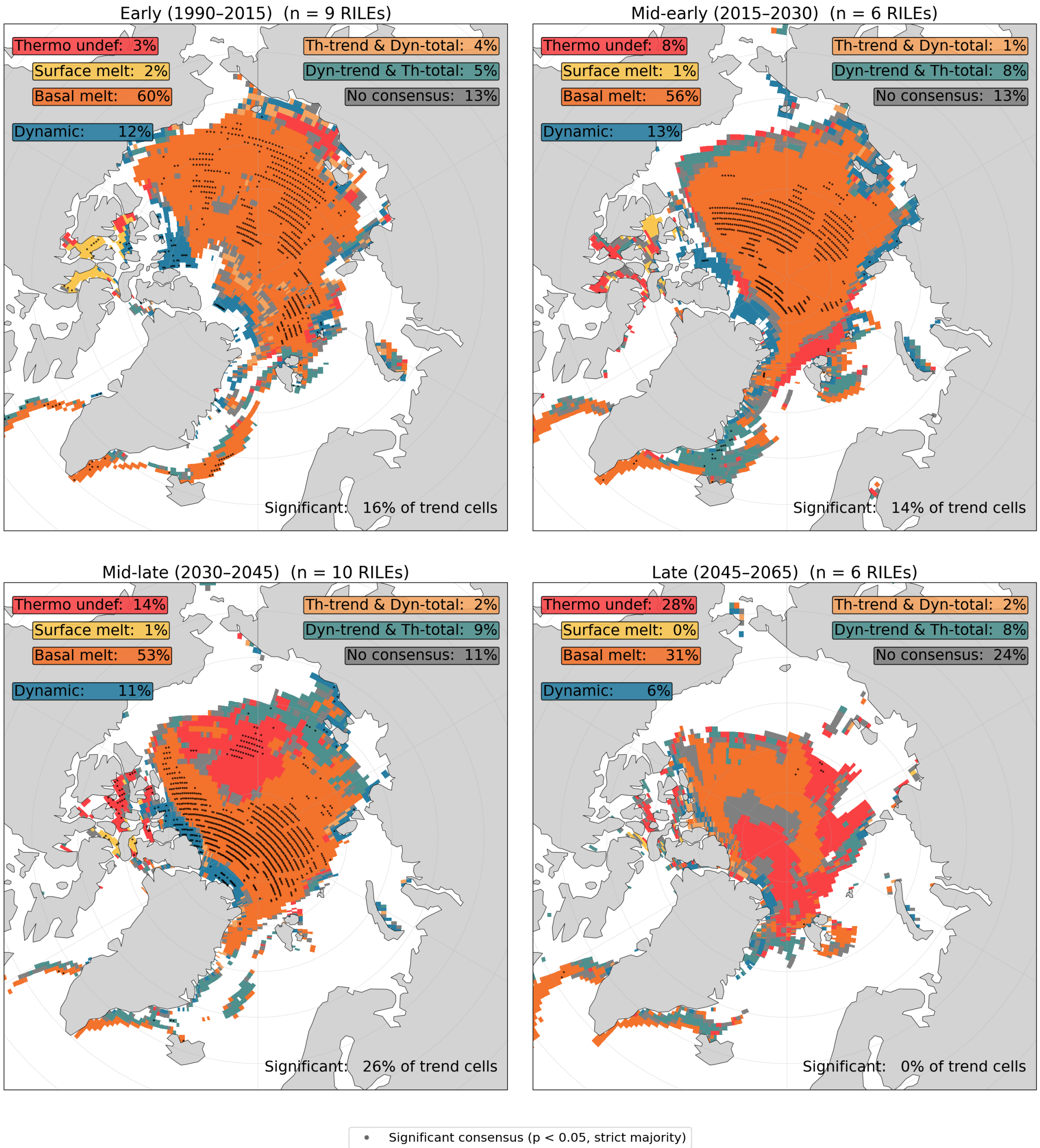

Figure 9. Same as Fig. 7, but based on sea ice mass tendencies. The thermodynamic category is further subdivided into surface ice melt and basal ice melt where consensus is reached, and left as thermodynamic undefined (red) otherwise. n denotes the number of RILEs in each period.

The sub-attribution maps (Fig. 9) confirm the dominant role of thermodynamic processes across all four periods, with basal melt emerging as the major driver of September sea ice decline during RILEs. Yet, the contribution of basal melt decreases, going from 60% in the early period to 31% in the late period. Dynamic processes account for a small but stable fraction of the diminishing ice pack, ranging from 6 to 13% of the area across the four periods. Surface melt plays a comparatively minor

https://doi.org/10.5194/egusphere-2026-4173
Preprint. Discussion started: 1 September 2026

role, with the fraction of attributed grid cells reaching a maximum of 2% across all periods. The mass-based reattribution stage reduces markedly the proportion of discordant grid cells relative to the main attribution, with the remaining discordant categories collectively accounting for approximately 9–11% of the declining sea ice area during RILEs. The sea ice mass budget therefore provides useful additional constraints for resolving ambiguous cases in the area-based decomposition. In contrast, the fractional area assigned to the no-consensus category, i.e. cells where two or more categories occur with equal frequency, increases slightly at the sub-attribution stage relative to the main attribution, which is consistent with the larger number of categories considered at this level. This fraction remains similar for the early, mid-early, and mid-late periods (12%, 13%, and 10%, respectively), but rises to 24% in the late period, likely reflecting the increased spatial variability of melt processes as the Arctic Ocean approaches nearly ice-free conditions.

The spatial distribution of the sub-attribution shows a shift in the dominant melt processes across the four RILE periods, transitioning from RILEs dominated by basal melt in the earliest period toward an increasingly complex interplay between basal and surface melt contributions in the later periods. In the early and mid-early periods, basal melt dominates continuously across the interior of the sea ice pack, while dynamic processes remain localised in the marginal ice zone. By the mid-late period, a region where both basal and surface melt contribute substantially to sea ice loss (Fig. 9) expands from the Beaufort and Chukchi Seas toward the central Arctic. Concurrently, the marginal ice zone in this period is characterised by grid cells where both thermodynamic and dynamic processes contribute to sea ice decline, while dynamic attribution remains prominent north of Greenland in the Lincoln Sea and in the vicinity of the Canadian Arctic Archipelago. In the late period, basal melt remains the dominant process (31% of trend cells), but the fraction of grid cells assigned to the undefined thermodynamic category, regions where neither basal nor surface melt can be identified as the primary driver, increases to 28%, concentrated in the central Arctic north of the Barents Sea. This spatial shift suggests that, as the sea ice cover thins and retreats toward the central Arctic, surface melt contributions during RILE periods become increasingly important.

Compared to the main attribution based on SIC changes, the fraction of grid cells exhibiting statistically significant frequency-based attribution decreases at the sub-attribution level in all periods except the mid-early one, where it increases from 10% to 15%. In the early and mid-late periods, the significant cells are predominantly attributed to basal melt, and also to dynamic processes localized in the Lincoln Sea close to the Greenland coast, indicating robust inter-RILE agreement on these dominant mechanisms. In the late period, the fraction of significant cells collapses from 31% in the main attribution to near zero at the sub-attribution level (Fig. 9), suggesting that, while thermodynamic processes are consistently identified as the dominant driver, the specific partitioning between basal and surface melt varies considerably across RILEs and cannot be robustly constrained given the small number of contributing events (n = 6) and the increased spatial heterogeneity of melt processes in a near-ice-free Arctic Ocean.

It is important to note that the dominance of basal melt in the attribution framework does not imply that surface melt plays no role in sea ice loss during RILEs. The seasonal cycle of sea ice mass budget components shows that surface melt contributes

https://doi.org/10.5194/egusphere-2026-4173
Preprint. Discussion started: 1 September 2026

meaningfully to sea ice loss from May to August across all four periods, with a consistent but secondary contribution relative to basal melt (Fig. S3). This confirms that surface processes are active during RILEs and cannot be dismissed as negligible, even though they do not emerge as the dominant driver in the attribution framework. Spatially, one might expect surface melt to dominate at lower latitudes within the Arctic domain, where solar insolation is strongest during summer, while basal melt would dominate on the Atlantic side and in the central Arctic, where oceanic heat storage and warm water intrusions provide sustained heat flux to the ice base. However, our results show that basal melt dominates across nearly the entire Arctic domain in all four periods, with the exception of the Canadian Archipelago.

4 Discussion

The improved representation of the Arctic sea ice state in CESM2-lessmelt simulations reveals that RILEs can occur throughout the entire 21st century, with a peak in probability around 2040 for September RILEs (Fig. 3). This temporal distribution implies that RILEs are not associated with a particular sea ice regime: they emerge under a wide range of mean states, from the comparatively extensive and thick ice cover of the 1990s and early 2000s to the markedly reduced and thinner ice conditions of the mid-century. This finding raises fundamental questions regarding the respective roles of preconditioning, externally forced change, and internal climate variability in triggering these events. Previous work using CCSM3 has shown that RILEs result from the combination of a thinning ice cover and a growing intrinsic variability in September SIE, with natural SIE variability playing a critical role in initiating individual events (Holland et al., 2008a). The occurrence of RILEs in CESM2-lessmelt as early as 1990–2015, when SIE variability is already higher than at the beginning of the 20th century yet the ice cover remains more extensive and thicker than in later periods, is consistent with this picture: internal variability alone appears sufficient to trigger rapid sea ice loss even in the early period. However, the dominant mechanisms likely differ across periods, as the mean sea ice state varies considerably. In the early period, changes in forcing variability and anomalous ocean heat transport may play a larger role (Holland et al., 2008a; DeRepentigny et al., 2020, 2022), while in later periods, the increased sensitivity of a thinner ice pack to internal variability may become the primary driver of rapid sea ice loss.

Internal variability represents a major source of uncertainty in projections of Arctic sea ice loss, particularly over the coming decades. As the ice cover thins under continued anthropogenic forcing, its sensitivity to internal climate fluctuations increases, such that natural variability can produce sea ice changes of a magnitude comparable to the externally forced signal (Holland et al., 2008a; Pasha Karami et al., 2023). Using a suite of single-model large ensembles, Bonan et al. (2021) showed that internal variability accounts for 40–60% of the total uncertainty in projections of September SIA change over the next decade, while scenario uncertainty only becomes dominant toward the end of the century. Furthermore, this contribution is state-dependent, increasing to approximately 80% of total uncertainty at low SIV regimes, consistent with the growing sensitivity of a thinner ice cover to internal climate perturbations (Bonan et al., 2021). In accordance with this, RILEs are a robust feature of future projections in the CESM2-lessmelt ensemble throughout the mid-early to late periods, reflecting the dominant role of internal variability over scenario uncertainty in driving rapid ice loss on decadal timescales. However, internal variability is not only

https://doi.org/10.5194/egusphere-2026-4173
Preprint. Discussion started: 1 September 2026

relevant towards the end of the 21st century. Pasha Karami et al. (2023) demonstrated that over 70% of the September SIA loss between the extreme high of 1996 and the extreme low of 2007 was attributable to internal variability, with half of this contribution arising from interdecadal modes. Consistently, the occurrence of RILEs in some CESM2-lessmelt members as early as the 1990s, as well as their occurrence in low-emission scenarios (Sticker et al., 2025), demonstrates that sufficiently large internal variability alone can trigger rapid ice loss even under moderate forcing relative to late 21st century levels.

A related question concerns whether the initial sea ice state influences RILE occurrence. In the CESM2-lessmelt ensemble, RILEs occur preferentially when the SIE of an individual member lies above the ensemble mean, though they are not excluded from occurring at or below it (Fig. 4). This raises the possibility that RILEs partly reflect a model tendency for members with anomalously high SIE to return toward the ensemble mean trajectory. However, the occurrence of RILEs at or below the ensemble mean demonstrates that this mechanism alone is insufficient to explain their full distribution, and that internal variability can trigger rapid sea ice loss independently of the initial sea ice state. RILEs therefore emerge across a range of initial sea ice conditions, reflecting the combined influence of external forcing, which sets the long-term thinning trajectory, and internal variability, which determines the timing and magnitude of individual events.

RILEs differ not only in their onset timing, and thus their initial sea ice state, but also in the intensity of their SIV loss trends throughout the event. For instance, RILEs in early and mid-early periods can exhibit a loss rate in SIV 3 to 4 times greater than that of RILEs in mid-late and late periods, suggesting that some of these events are not solely driven by areal changes but also involve changes in ice thickness (Fig. 5). This result led us to further investigate the behavior of SIT distribution during these rapid melt events. The results discussed above highlight that SIA alone provides an incomplete picture of the physical changes occurring during these events. As noted by Stroeve and Notz (2018) and Massonnet et al. (2018), the stability of the Arctic sea ice cover is closely tied to the thickness distribution of the ice pack: a thicker, more heterogeneous ice cover responds differently to thermodynamic forcing than a thin, homogeneous one, with compensating negative feedbacks, such as enhanced winter ice growth in areas that became ice-free during summer, playing a key role in stabilizing the system. As the ice pack thins under continued warming, these stabilizing feedbacks weaken, and the nature of RILEs could change fundamentally.

Analysis of the fractional SIA by thickness category revealed distinct redistribution patterns during RILEs. In the early period, the initial thickness distribution is relatively uniform across the five model thickness categories. By the end of the events, the total SIA has declined by approximately 2 million km^2 on average over RILE durations of 5 to 8 years. This areal loss is primarily driven by the reduction of the thickest ice categories (>2.47m), while the area of the thinnest ice (0–0.64 m) remains approximately constant or increases in absolute values, with its fractional contribution to the total SIA more than doubling in some cases. A similar pattern emerges in RILES of the mid-early period, though it initiates with a higher proportion of thin ice categories. In contrast, in the last two periods, RILEs do not exhibit significant thickness redistribution; instead, they are primarily characterized by the decline of thin ice. This highlights the distinct nature of RILEs: early-century events not only reduce total ice area and volume but also redistribute ice from thick to thin categories, whereas mid-century events primarily

https://doi.org/10.5194/egusphere-2026-4173
Preprint. Discussion started: 1 September 2026

eliminate thin ice.

To further understand how RILEs develop, we characterized sea ice loss during RILEs in terms of its driving processes for the first time. The Arctic sea ice state is governed by a balance between thermodynamic (sea ice melt/growth) and dynamic (sea ice import/export) contributions (Holland et al., 2008b). We found that negative trends in September SIC strongly correlate (r = 0.89–0.93) with total SIC melt trends, confirming that September sea ice conditions largely reflect melt-season processes. In CESM2 model, SIC changes can be decomposed into dynamic and thermodynamic components, enabling a first attribution of SIC loss to these processes, initially based on areal dimensions. Our results show that thermodynamic processes dominate sea ice concentration decline across all four RILEs period, accounting for 39–69% of the area affected by sea ice loss, while dynamic processes contribute 5–11%. The remaining fraction of the SIA decline occurs in regions where no single process emerges as dominant. Previous studies have identified thermodynamic processes as the primary driver of rapid Arctic sea ice loss, with dynamic processes playing a negligible direct role (Holland et al., 2006; Döscher and Koenigk, 2013). Regions where no single process dominates in the attribution analysis are likely regions where comparable contributions from both thermodynamic and dynamic processes occur, or where the signal in the process attribution is less clear. This ambiguity in attribution often arises in areas with minimal or near-zero sea ice trends (not shown). Analysis of the distribution of September SIC trends by attribution category confirms that discordant regions are predominantly associated with slight to moderate sea ice loss, while the most strongly negative trends are predominantly found in thermodynamically dominated regions (Fig. 8).

While concentration-based attribution already provides insight into the processes driving sea ice loss during RILEs, a complementary mass-based analysis further confirms the dominant role of thermodynamic processes, expanding the fraction of sea ice loss regions attributed to thermodynamic forcing. Within this thermodynamic contribution, basal melt consistently emerges as the dominant mechanism of sea ice loss across all RILEs. This dominance likely reflects the combined action of two mechanisms: the ice-albedo feedback, through which expanding open-water areas increase solar heat absorption in the upper ocean, and reorganizations of ocean circulation and associated heat transport, both of which enhance oceanic heat flux to the ice base and drive basal melt.

For the early period, however, the ice-albedo feedback is less likely to explain the RILEs. Occurring when the Arctic Ocean is still largely covered by thick, extensive sea ice, the contribution of solar radiation absorbed through leads is likely minimal. It is worth noting that the early period coincides with a period of enhanced variability in biomass burning (BB) emissions identified in CESM2 (DeRepentigny et al., 2022). That study attributes the enhanced simulated adecline in September sea ice between 1997 and 2014 to this increased BB variability, driven by nonlinear aerosol–cloud interactions: years with low BB-related aerosol burdens reduce cloud optical depth and produce a warming effect that outweighs the cooling induced during years with high aerosol burdens, resulting in a net warming of the surface. This highlights the sensitivity of Arctic sea ice to aerosol emission variability. However, the fact that four members using a smoothed BB emission forcing still exhibit RILEs

https://doi.org/10.5194/egusphere-2026-4173
Preprint. Discussion started: 1 September 2026

during this early period indicates that such events are not solely attributable to this aerosol forcing.

Finally, for the RILE in the latest period in the century, large regions near the ice edge exhibit ambiguous attribution between surface and basal melt. This ambiguity may indicate that, by this period, atmospheric warming has become sufficient to drive surface melt rates comparable to those of basal melt, or alternatively, that other thermodynamic mechanisms such as lateral melt have gained relative importance at a spatial scale. Regarding the late period, the six RILEs identified all result in September SIE reaching Arctic Ocean ice-free conditions. This is consistent with previous studies showing that early ice-free days always occur during rapid ice loss events (Heuzé and Jahn, 2024), and that around a third of RILEs in Sticker et al. (2025) study lead to seasonally ice-free conditions, suggesting that RILEs are important role in the transition toward a seasonally ice-free Arctic Ocean.

These findings are consistent with the causal analysis of Docquier et al. (2024), who demonstrate using the Liang-Kleeman information flow method that surface air temperature is the dominant driver of summer Arctic SIE across five CMIP6 large ensembles, with its influence being particularly pronounced during periods of rapid sea ice decline. This supports the thermodynamic dominance identified here, though our results further suggest that this atmospheric forcing acts primarily through basal melt rather than surface melt, pointing to ocean heat uptake as the key intermediary between atmospheric warming and sea ice loss during RILEs. Furthermore, we also showed a strengthening of the thermodynamic-severity in SIC decline coupling from the early to the late period. Docquier et al. (2024) show that the causal influence of surface air temperature on summer SIE increases over time in conjunction with a growing frequency of sea ice lows and rapid sea ice decline events.

The dominance of basal ice melt in the attribution framework should not be interpreted as finding an absence of surface melt during RILEs. The seasonal cycle of sea ice mass budget components shows that surface melt contributes meaningfully to sea ice loss from May to August across all periods, albeit as a secondary process relative to basal melt (Fig. S3). The thermodynamic dominance of basal melt therefore reflects the primary mechanism of the most intense and spatially coherent sea ice loss during RILEs, rather than the exclusive process at play. Moreover, both models and observations consistently point toward an increasing dominance of basal melt over surface melt in the Arctic sea ice mass budget, suggesting that the basal melt dominance identified here is consistent with the broader literature (Carmack et al., 2015; Keen et al., 2021; Richaud et al., 2026).

5 Conclusions

The accelerating loss of Arctic summer sea ice represents one of the most striking manifestations of ongoing climate change, with thermodynamic and dynamic processes jointly shaping the pace and spatial pattern of this decline. Using the CESM2-lessmelt ensemble under the SSP3-7.0 scenario, we showed that RILEs are a robust and recurrent feature of Arctic sea ice evolution throughout 1990–2065, with a peak in occurrence around 2040. Their distribution across the full simulation period from the historical era, where the forced signal remains modest, to the mid-to-late 21st century, where a thinning ice cover amplifies the role of internal variability, underscores the dual nature of their triggering: externally forced thinning sets the background conditions, while internal variability provides the perturbation necessary to initiate individual events. Our two-stage attribution framework revealed that thermodynamic sea ice processes dominate SIA loss during RILEs across all four periods, accounting for 46–71% of attributed grid cells, while dynamic sea ice processes contribute a consistently minor fraction of 6–11%. A further decomposition of the thermodynamic signal identified basal melt as the primary driver, with its relative contribution decreasing from the early (64%) to the late period (32%) as the ice cover thins and surface melt becomes increasingly relevant.

A more complete characterisation of RILE evolution would require a detailed investigation of their precursors, including atmospheric and oceanic preconditioning, surface energy budget feedbacks, and remote climate drivers. Advanced understanding of the ocean–ice–atmosphere interactions driving these rapid sea ice decline is essential to reduce uncertainties in projections of Arctic sea ice loss and its broader climatic consequences. Further work combining modeling, observational constraints on basal and surface ice melt, and large ensemble approaches will be critical to refining our understanding of the mechanisms behind those Arctic RILEs in a warming world and ultimately to developing reliable early warning systems of imminent rapid loss events, with important implications for Arctic ecosystem management, shipping route planning, and climate adaptation strategies.

Data availability. CESM2-LE data are available here: https://www.cesm.ucar.edu/projects/community-projects/LENS2/. The CESM2-lessmelt data are available via Globus access to NCAR GLADE at: */glade/campaign/cgd/ppc/cesm2_tuned_albedo* (Kay et al., 2022). The observational SIE data from the National Snow and Ice Data Center (NSIDC) can be accessed via https://nsidc.org/data/nsidc-0192/versions/3.

Author contributions. AS, FM, TF and AJ conceptualized the science plan. AS performed the analyses, produced the figures and wrote the manuscript based on the insights from the co-authors. AS, BR, AJ, FM, DB and TF contributed to writing, reviewing, and editing.

Competing interests. The authors declare that they have no conflict of interest.

Acknowledgements. Annelies Sticker is funded by the European Union (ERC, ArcticWATCH, 101040858). Views and opinions expressed are however those of the author(s) only and do not necessarily reflect those of the European Union or the European Research Council Executive Agency. Neither the European Union nor the granting authority can be held responsible for them. François Massonnet is a F.R.S.-FNRS Research Associate. Computational resources have been provided by the supercomputing facilities of the Université catholique de

https://doi.org/10.5194/egusphere-2026-4173
Preprint. Discussion started: 1 September 2026

Louvain (CISM/UCL) and the Consortium des Équipements de Calcul Intensif en Fédération Wallonie Bruxelles (CÉCI) funded by the Fond de la Recherche Scientifique de Belgique (F.R.S.–FNRS) under convention 2.5020.11. We also acknowledge usage of NCAR's Casper system (https://ncar.pub/casper) for initial data analysis, which is sponsored by the National Science Foundation. A. Jahn's contribution was funded by NSF-CAREER award 1847398. Annelies Sticker gratefully acknowledges financial support for this research by the Fulbright U.S. Student Program, which is sponsored by the U.S. Department of State and the Fulbright Belgium Program. Its contents are solely the responsibility of the author and do not necessarily represent the official views of the Fulbright Program, the Government of the United States, or the Fulbright Belgium Program. The authors used Claude (Anthropic) to assist with language editing and improving the clarity of the manuscript.

References

Arrigo, K. R. and van Dijken, G. L.: Secular trends in Arctic Ocean net primary production, Journal of Geophysical Research: Oceans, 116, https://doi.org/https://doi.org/10.1029/2011JC007151, 2011.

Auclair, G. and Tremblay, L. B.: The Role of Ocean Heat Transport in Rapid Sea Ice Declines in the Community Earth System Model Large Ensemble, Journal of Geophysical Research: Oceans, 123, 8941–8957, https://doi.org/10.1029/2018JC014525, _eprint: https://onlinelibrary.wiley.com/doi/pdf/10.1029/2018JC014525, 2018.

Baxter, I., Ding, Q., Schweiger, A., L'Heureux, M., Baxter, S., Wang, T., Zhang, Q., Harnos, K., Markle, B., Topal, D., and Lu, J.: How Tropical Pacific Surface Cooling Contributed to Accelerated Sea Ice Melt from 2007 to 2012 as Ice Is Thinned by Anthropogenic Forcing, Journal of Climate, 32, 8583 – 8602, https://doi.org/10.1175/JCLI-D-18-0783.1, 2019.

Bitz, C. M., Holland, M. M., Weaver, A. J., and Eby, M.: Simulating the ice-thickness distribution in a coupled climate model, Journal of Geophysical Research: Oceans, 106, 2441–2463, https://doi.org/https://doi.org/10.1029/1999JC000113, 2001.

Bonan, D., Lehner, F., and Holland, M.: Partitioning uncertainty in projections of Arctic sea ice, Environmental Research Letters, https://doi.org/10.1088/1748-9326/abe0ec, 2021.

Bushuk, M., Winton, M., Bonan, D. B., Blanchard-Wrigglesworth, E., and Delworth, T. L.: A Mechanism for the Arctic Sea Ice Spring Predictability Barrier, Geophysical Research Letters, 47, e2020GL088 335, https://doi.org/https://doi.org/10.1029/2020GL088335, e2020GL088335 10.1029/2020GL088335, 2020.

Carmack, E., Polyakov, I., Padman, L., Fer, I., Hunke, E., Hutchings, J., Jackson, J., Kelley, D., Kwok, R., Layton, C., Melling, H., Perovich, D., Persson, O., Ruddick, B., Timmermans, M.-L., Toole, J., Ross, T., Vavrus, S., and Winsor, P.: Toward Quantifying the Increasing Role of Oceanic Heat in Sea Ice Loss in the New Arctic, Bulletin of the American Meteorological Society, 96, 2079 – 2105, https://doi.org/10.1175/BAMS-D-13-00177.1, 2015.

Cohen, J., Zhang, X., Francis, J., Jung, T., Kwok, R., Overland, J., Ballinger, T., Bhatt, U., Chen, H., Coumou, D., Feldstein, S., Gu, H., Handorf, D., Henderson, G., Ionita, M., Kretschmer, M., Laliberté, F., Lee, S., Linderholm, H., and Yoon, J.-H.: Divergent consensuses on Arctic amplification influence on midlatitude severe winter weather, Nature Climate Change, 10, 1–10, https://doi.org/10.1038/s41558-019-0662-y, 2019.

Danabasoglu, G., Lamarque, J.-F., Bacmeister, J., Bailey, D. A., DuVivier, A. K., Edwards, J., Emmons, L. K., Fasullo, J., Garcia, R., Gettelman, A., Hannay, C., Holland, M. M., Large, W. G., Lauritzen, P. H., Lawrence, D. M., Lenaerts, J. T. M., Lindsay, K., Lipscomb, W. H., Mills, M. J., Neale, R., Oleson, K. W., Otto-Bliesner, B., Phillips, A. S., Sacks, W., Tilmes, S., van Kampenhout, L., Vertenstein, M., Bertini, A., Dennis, J., Deser, C., Fischer, C., Fox-Kemper, B., Kay, J. E., Kinnison, D., Kushner, P. J., Larson, V. E., Long, M. C., Mickelson, S., Moore, J. K., Nienhouse, E., Polvani, L., Rasch, P. J., and Strand, W. G.: The Community Earth System Model Version 2 (CESM2), Journal of Advances in Modeling Earth Systems, 12, e2019MS001 916, https://doi.org/https://doi.org/10.1029/2019MS001916, 2020.

Delhaye, S., Msadek, R., Fichefet, T., Massonnet, F., and Terray, L.: Consistent but more intense atmospheric circulation response to Arctic sea ice loss in CMIP6 experiments compared to PAMIP experiments, EGUsphere, 2023, 1–32, https://doi.org/10.5194/egusphere-2023-1748, 2023.

DeRepentigny, P., Jahn, A., Holland, M. M., and Smith, A.: Arctic Sea Ice in Two Configurations of the CESM2 During the 20th and 21st Centuries, Journal of Geophysical Research: Oceans, 125, e2020JC016 133, https://doi.org/https://doi.org/10.1029/2020JC016133, e2020JC016133 10.1029/2020JC016133, 2020.

DeRepentigny, P., Jahn, A., Holland, M. M., Kay, J. E., Fasullo, J., Lamarque, J.-F., Tilmes, S., Hannay, C., Mills, M. J., Bailey, D. A., and Barrett, A. P.: Enhanced simulated early 21st century Arctic sea ice loss due to CMIP6 biomass burning emissions, Science Advances, 8, eabo2405, https://doi.org/10.1126/sciadv.abo2405, 2022.

Ding, Q., Wallace, J., Battisti, D., Steig, E., Gallant, A., Kim, H.-J., and Geng, L.: Tropical forcing of the recent rapid Arctic warming in Northeastern Canada and Greenland, Nature, 509, 209–12, https://doi.org/10.1038/nature13260, 2014.

Docquier, D., Massonnet, F., Ragone, F., Sticker, A., Fichefet, T., and Vannitsem, S.: Drivers of summer Arctic sea-ice extent at interannual time scale in CMIP6 large ensembles revealed by information flow, Scientific Reports, 14, https://doi.org/10.1038/s41598-024-76056-y, 2024.

DuVivier, A. K., Holland, M. M., Kay, J. E., Tilmes, S., Gettelman, A., and Bailey, D. A.: Arctic and Antarctic Sea Ice Mean State in the Community Earth System Model Version 2 and the Influence of Atmospheric Chemistry, Journal of Geophysical Research: Oceans, 125, e2019JC015 934, https://doi.org/https://doi.org/10.1029/2019JC015934, 2020.

Döscher, R. and Koenigk, T.: Arctic rapid sea ice loss events in regional coupled climate scenario experiments, Ocean Science, 9, 217–248, https://doi.org/10.5194/os-9-217-2013, 2013.

Fasullo, J. T., Lamarque, J.-F., Hannay, C., Rosenbloom, N., Tilmes, S., DeRepentigny, P., Jahn, A., and Deser, C.: Spurious Late Historical-Era Warming in CESM2 Driven by Prescribed Biomass Burning Emissions, Geophysical Research Letters, 49, e2021GL097 420, https://doi.org/https://doi.org/10.1029/2021GL097420, 2022.

Fetterer, F., Knowles, K., Meier, W., Savoie, M., and Windnagel, A.: Sea Ice Index, Version 3 [monthly values from 1979 to 2023], https://doi.org/10.7265/N5K072F8, accessed Apr 2024, 2017.

Goosse, H., Arzel, O., Bitz, C. M., de Montety, A., and Vancoppenolle, M.: Increased variability of the Arctic summer ice extent in a warmer climate, Geophysical Research Letters, 36, L23 702, https://doi.org/10.1029/2009GL040546, 2009.

Guern-Lepage, A. and Tremblay, B.: Disentangling Dynamic from Thermodynamic Summer Ice Area Loss from Observations (1979–2021): A Potential Mechanism for a "First-Time" Ice-Free Arctic, Journal of Climate, 36, 7693–7713, https://doi.org/10.1175/JCLI-D-22-0628.1, 2023.

Heuzé, C. and Jahn, A.: The first ice-free day in the Arctic Ocean could occur before 2030, Nature Communications, 15, https://doi.org/10.1038/s41467-024-54508-3, 2024.

Holland, M., Bitz, C., Tremblay, B., and Bailey, D.: The Role of Natural Versus Forced Change in Future Rapid Summer Arctic Ice Loss, Washington DC American Geophysical Union Geophysical Monograph Series, 180, https://doi.org/10.1029/180GM10, 2008a.

Holland, M., Serreze, M., and Stroeve, J.: The sea ice mass budget of the Arctic and its future change as simulated by coupled climate models, Climate Dynamics, 34, 185–200, https://doi.org/10.1007/s00382-008-0493-4, 2008b.

Holland, M. M., Bitz, C. M., and Tremblay, B.: Future abrupt reductions in the summer Arctic sea ice, Geophysical Research Letters, 33, https://doi.org/10.1029/2006GL028024, 2006.

Hunke, E. C., Hebert, D. A., and Lecomte, O.: Level-ice melt ponds in the Los Alamos sea ice model, CICE, Ocean Modelling, 71, 26–42, https://doi.org/https://doi.org/10.1016/j.ocemod.2012.11.008, arctic Ocean, 2013.

Kay, J., Holland, M., and Jahn, A.: Inter-annual to multi-decadal Arctic sea ice extent trends in a warming world, Geophysical Research Letters, 38, L15 708, https://doi.org/10.1029/2011GL048008, 2011.

Kay, J. E., DeRepentigny, P., Holland, M. M., Bailey, D. A., DuVivier, A. K., Blanchard-Wrigglesworth, E., Deser, C., Jahn, A., Singh, H., Smith, M. M., Webster, M. A., Edwards, J., Lee, S.-S., Rodgers, K. B., and Rosenbloom, N.: Less Surface Sea Ice Melt in the CESM2

Improves Arctic Sea Ice Simulation With Minimal Non-Polar Climate Impacts, Journal of Advances in Modeling Earth Systems, 14, e2021MS002 679, https://doi.org/https://doi.org/10.1029/2021MS002679, e2021MS002679 2021MS002679, 2022.

Keen, A. and Blockley, E.: Investigating future changes in the volume budget of the Arctic sea ice in a coupled climate model, The Cryosphere, 12, 2855–2868, https://doi.org/10.5194/tc-12-2855-2018, 2018.

Keen, A., Blockley, E., Bailey, D. A., Boldingh Debernard, J., Bushuk, M., Delhaye, S., Docquier, D., Feltham, D., Massonnet, F., O'Farrell, S., Ponsoni, L., Rodriguez, J. M., Schroeder, D., Swart, N., Toyoda, T., Tsujino, H., Vancoppenolle, M., and Wyser, K.: An inter-comparison of the mass budget of the Arctic sea ice in CMIP6 models, The Cryosphere, 15, 951–982, https://doi.org/10.5194/tc-15-951-2021, 2021.

Lawrence, D., Slater, A., Tomas, R., Holland, M., and Deser, C.: Accelerated Arctic land warming and permafrost degradation during rapid sea ice loss, AGU Fall Meeting Abstracts, 35, https://doi.org/10.1029/2008GL033985, 2008.

Lipscomb, W. H.: Remapping the thickness distribution in sea ice models, Journal of Geophysical Research: Oceans, 106, 13 989–14 000, https://doi.org/https://doi.org/10.1029/2000JC000518, 2001.

Massonnet, F., Fichefet, T., Goosse, H., Bitz, C. M., Philippon-Berthier, G., Holland, M. M., and Barriat, P.-Y.: Constraining projections of summer Arctic sea ice, The Cryosphere, 6, 1383–1394, https://doi.org/10.5194/tc-6-1383-2012, 2012.

Massonnet, F., Vancoppenolle, M., Goosse, H., Docquier, D., Fichefet, T., and Blanchard-Wrigglesworth, E.: Arctic sea-ice change tied to its mean state through thermodynamic processes, Nature Climate Change, 8, https://doi.org/10.1038/s41558-018-0204-z, 2018.

McIlhattan, E. and L'Ecuyer, T.: Improved Arctic Near-Surface Air Temperatures in CESM2 Relative to Surface Station and Buoy Measurements, Journal of Climate, 38, 4589–4610, https://doi.org/10.1175/JCLI-D-24-0046.1, 2025.

Meredith, M., Sommerkorn, M., Cassotta, S., Derksen, C., Ekaykin, A., Hollowed, A., Kofinas, G., Mackintosh, A., Melbourne-Thomas, J., Muelbert, M., Ottersen, G., Pritchard, H., and Schuur, E.: Polar Regions, in: IPCC Special Report on the Ocean and Cryosphere in a Changing Climate, edited by Pörtner, H.-O., Roberts, D., Masson-Delmotte, V., Zhai, P., Tignor, M., Poloczanska, E., Mintenbeck, K., Alegrí´a, A., Nicolai, M., Okem, A., Petzold, J., Rama, B., and NM, W., pp. 203–320, Cambridge University Press, Cambridge, UK and New York, NY, USA, 2019.

Mioduszewski, J. R., Vavrus, S., Wang, M., Holland, M., and Landrum, L.: Past and future interannual variability in Arctic sea ice in coupled climate models, The Cryosphere, 13, 113–124, https://doi.org/10.5194/tc-13-113-2019, 2019.

Paquin, J.-P., Döscher, R., Sushama, L., and Koenigk, T.: Causes and consequences of mid–21st-century rapid ice loss events simulated by the Rossby centre regional atmosphere-ocean model, Tellus A: Dynamic Meteorology and Oceanography, 65, 19 110, https://doi.org/10.3402/tellusa.v65i0.19110, 2013.

Pasha Karami, M., Koenigk, T., and Tremblay, B.: Variability of summer-time Arctic sea ice: the drivers and the contribution to the sea ice trend and extremes, Environmental Research Climate, 2, https://doi.org/10.1088/2752-5295/accbe3, 2023.

Polyakov, I. V., Pnyushkov, A. V., Alkire, M. B., Ashik, I. M., Baumann, T. M., Carmack, E. C., Goszczko, I., Guthrie, J., Ivanov, V. V., Kanzow, T., Krishfield, R., Kwok, R., Sundfjord, A., Morison, J., Rember, R., and Yulin, A.: Greater role for Atlantic inflows on sea-ice loss in the Eurasian Basin of the Arctic Ocean, Science, 356, 285–291, https://doi.org/10.1126/science.aai8204, 2017.

Polyakov, I. V., Mayer, M., Tietsche, S., and Karpechko, A. Y.: Climate Change Fosters Competing Effects of Dynamics and Thermodynamics in Seasonal Predictability of Arctic Sea Ice, Journal of Climate, 35, 2849 – 2865, https://doi.org/10.1175/JCLI-D-21-0463.1, 2022.

Post, E., Bhatt, U., Bitz, C., Brodie, J., Fulton, T., Hebblewhite, M., Kerby, J., Stirling, I., and Walker, D.: Ecological Consequences of Sea-Ice Decline, Science (New York, N.Y.), 341, 519–24, https://doi.org/10.1126/science.1235225, 2013.

https://doi.org/10.5194/egusphere-2026-4173
Preprint. Discussion started: 1 September 2026

Richaud, B., Massonnet, F., Fichefet, T., Topál, D., Barthélemy, A., and Docquier, D.: Anatomy of Arctic and Antarctic sea ice lows in an ocean–sea ice model, The Cryosphere, 20, 791–810, https://doi.org/10.5194/tc-20-791-2026, 2026.

Rieke, O., Årthun, M., and Dörr, J. S.: Rapid sea ice changes in the future Barents Sea, The Cryosphere, 17, 1445–1456, https://doi.org/10.5194/tc-17-1445-2023, 2023.

Rodgers, K. B., Lee, S.-S., Rosenbloom, N., Timmermann, A., Danabasoglu, G., Deser, C., Edwards, J., Kim, J.-E., Simpson, I. R., Stein, K., Stuecker, M. F., Yamaguchi, R., Bódai, T., Chung, E.-S., Huang, L., Kim, W. M., Lamarque, J.-F., Lombardozzi, D. L., Wieder, W. R., and Yeager, S. G.: Ubiquity of human-induced changes in climate variability, Earth System Dynamics, 12, 1393–1411, https://doi.org/10.5194/esd-12-1393-2021, 2021.

Rogers, T. S., Walsh, J. E., Leonawicz, M., and Lindgren, M.: Arctic sea ice: use of observational data and model hindcasts to refine future projections of ice extent, Polar Geography, 38, 22–41, https://doi.org/10.1080/1088937X.2014.987849, 2015.

Schweiger, A., Lindsay, R., Zhang, J., Steele, M., Stern, H., and Kwok, R.: Uncertainty in modeled Arctic sea ice volume, JOURNAL OF GEOPHYSICAL RESEARCH-OCEANS, 116, https://doi.org/10.1029/2011JC007084, 2011.

Serreze, M. C., Crawford, A. D., Stroeve, J. C., Barrett, A. P., and Woodgate, R. A.: Variability, trends, and predictability of seasonal sea ice retreat and advance in the Chukchi Sea, Journal of Geophysical Research: Oceans, 121, 7308–7325, https://doi.org/10.1002/2016JC011977, 2016.

Sticker, A. et al.: Seasonality and scenario dependence of rapid Arctic sea ice loss events in CMIP6 simulations, The Cryosphere, 19, 3259–3277, https://doi.org/https://doi.org/10.5194/tc-19-3259-2025, 2025.

Stroeve, J. and Notz, D.: Insights on past and future sea-ice evolution from combining observations and models, Global and Planetary Change, 135, https://doi.org/10.1016/j.gloplacha.2015.10.011, 2015.

Stroeve, J. and Notz, D.: Changing state of Arctic sea ice across all seasons, Environmental Research Letters, 13, 103 001, https://doi.org/10.1088/1748-9326/aade56, 2018.

Sumata, H., de Steur, L., Divine, D. V., Granskog, M. A., and Gerland, S.: Regime shift in Arctic Ocean sea ice thickness, Nature, 615, 443–449, https://doi.org/10.1038/s41586-022-05686-x, 2023.

Swart, N. C., Fyfe, J. C., Hawkins, E., Kay, J. E., and Jahn, A.: Influence of internal variability on Arctic sea-ice trends, Nature Climate Change, 5, 86–89, https://doi.org/10.1038/nclimate2483, number: 2 Publisher: Nature Publishing Group, 2015.

Vavrus, S., Holland, M., and Bailey, D.: Changes in Arctic clouds during intervals of rapid sea ice loss, Climate Dynamics, 36, 1475–1489, https://doi.org/10.1007/s00382-010-0816-0, 2011.

Wang, Q., Wekerle, C., Wang, X., Danilov, S., Koldunov, N., Sein, D., Sidorenko, D., von Appen, W.-J., and Jung, T.: Intensification of the Atlantic Water Supply to the Arctic Ocean Through Fram Strait Induced by Arctic Sea Ice Decline, Geophysical Research Letters, https://doi.org/10.1029/2019GL086682, 2020.

Wassmann, P., Duarte, C. M., Agusti, S., and Sejr, M. K.: Footprints of climate change in the Arctic marine ecosystem, Global Change Biology, 17, 1235–1249, https://doi.org/https://doi.org/10.1111/j.1365-2486.2010.02311.x, 2011.

Årthun, M., Eldevik, T., and Smedsrud, L. H.: The Role of Atlantic Heat Transport in Future Arctic Winter Sea Ice Loss, Journal of Climate, 32, 3327 – 3341, https://doi.org/10.1175/JCLI-D-18-0750.1, 2019.